Molecular and Dimensional Profiling of Highly Purified Extracellular Vesicles by Fluorescence Fluctuation Spectroscopy

ARTICLE *in* ANALYTICAL CHEMISTRY · JULY 2014

Impact Factor: 5.64 · DOI: 10.1021/ac501801m · Source: PubMed

6 AUTHORS, INCLUDING:

Romain Wyss
École Polytechnique Fédérale de Lausanne
13 PUBLICATIONS **124** CITATIONS
SEE PROFILE

Luigino Grasso
École Polytechnique Fédérale de Lausanne
10 PUBLICATIONS **90** CITATIONS
SEE PROFILE

Camille Wolf
École Polytechnique Fédérale de Lausanne
1 PUBLICATION **3** CITATIONS
SEE PROFILE

Wolfgang Grosse
CureVac
7 PUBLICATIONS **49** CITATIONS
SEE PROFILE

analytical chemistry

Letter

pubs.acs.org/ac

Molecular and Dimensional Profiling of Highly Purified Extracellular Vesicles by Fluorescence Fluctuation Spectroscopy

Romain Wyss,[§,#] Luigino Grasso,[§,#] Camille Wolf,[§] Wolfgang Grosse,[§] Davide Demurtas,[‡] and Horst Vogel*[,§]

[§]Laboratory of Physical Chemistry of Polymers and Membranes, Ecole Polytechnique Fédérale de Lausanne, Station 6, 1015 Lausanne, Switzerland

[‡]Interdisciplinary Center for Electron Microscopy, Ecole Polytechnique Fédérale de Lausanne, Station 12, 1015 Lausanne, Switzerland

Supporting Information

ABSTRACT: Cells secrete extracellular vesicles (EVs) into their microenvironment that act as mediators of intercellular communication under physiological conditions and in this context also actively participate in spreading various diseases. Large efforts are currently made to produce reliable EV samples and to develop, improve, and standardize techniques allowing their biophysical characterization. Here, we used ultrafiltration and size-exclusion chromatography for the isolation and a model-free fluorescence fluctuation analysis for the investigation of the physical and biological properties of EVs secreted by mammalian cells. Our purification strategy produced enriched samples of morphologically intact EVs free of extravesicular proteins and allowed labeling of marker molecules on the vesicle surface for single-vesicle analysis with single-molecule sensitivity. This novel approach provides information on the distribution profile of both EV size and relative expression level of a specific exosomal marker, deciphering the overall heterogeneity of EV preparations.

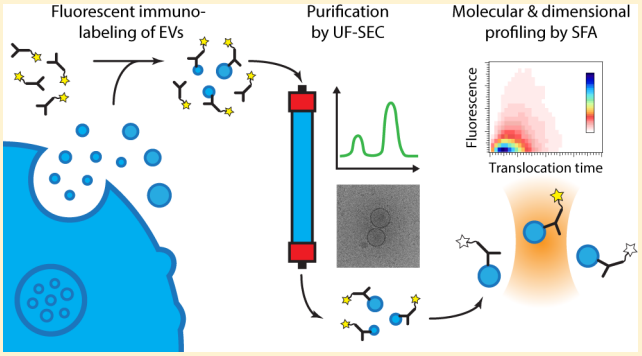

Extracellular vesicles (EVs) are nano- to micrometer-sized containers secreted by cells as membrane enclosed volumes comprising cellular components like proteins and nucleic acids. There are two main vesicle families: (i) *Exosomes* are unilamellar vesicles of 30 to 100 nm diameter released from a cell into the extracellular environment by the fusion of intracellular, multivesicular bodies (MVBs) with the cell's plasma membrane. (ii) *Microvesicles* are directly derived by an exocytotic process from the cell's plasma membrane and vary in diameters from hundreds to thousands of nanometers. EVs are naturally present in body fluids and carry chemical information for intercellular communication by activating signaling cascades in or delivering bioactive molecules such as lipids, proteins, or RNAs to the target cells.[1,2] There is increasing evidence that EVs play a central role in the development of diverse pathologies such as cancer,[3] and inflammatory[4] and neurodegenerative diseases,[5] with high potential to be used as biomarkers[3] and therapeutic agents.[6] Reliable biophysical/bioanalytical investigation of EVs (origin, subtypes, size, cargo) has thus become an important challenge considering the EVs' large heterogeneity in size and molecular composition and the difficulty in reproducibly isolating and purifying EVs from cultured cells or biological fluids. Currently, EVs are isolated by different techniques including filtration,[7,8] liquid chromatography,[9,10] microfluidics,[11,12] and differential ultracentrifugation;[13,14] the latter, offering in addition vesicle upconcentration, is the most employed method. However, large efforts remain to be undertaken to standardize the isolation of EVs as protocols used up until now are bewildering diverse.[15] An ideal procedure should deliver highly purified EVs without physical damage or aggregation while maximizing the yield and minimizing sample volume and handling time. Here, we combined ultrafiltration (UF) with size-exclusion chromatography (SEC) to first enrich an immunofluorescently labeled EV population and subsequently remove contaminants such as soluble proteins and unbound fluorescent antibodies, leading to highly concentrated and pure EV solutions for further molecular and dimensional profiling. Electron microscopy, flow cytometry, nanoparticle tracking analysis, and dynamic light scattering represent the most widely used tools for the study of EVs,[16,17] each of these methodologies presenting particular detection limits on the vesicles' size, concentration, or labeling. Intensity-based analysis using fluorescence microscopy was also proposed to determine size distribution of artificial lipid vesicles.[18] Surprisingly, fluorescence correlation spectroscopy (FCS) has not yet been employed for the detection and characterization of EVs. This

Received: May 12, 2014
Accepted: July 7, 2014
Published: July 7, 2014

   dx.doi.org/10.1021/ac501801m | *Anal. Chem.* 2014, 86, 7229−7233

technique is based on the analysis of fluctuations in a fluorescence signal produced by single fluorescent probes that diffuse through a confocal excitation/detection volume.[19,20] For instance, FCS enables one to decipher biomolecular interactions,[21] to monitor molecular diffusions on/in the plasma membrane,[22] and to investigate photochemical properties of fluorescent probes[23] by applying various models to fit the autocorrelation function (ACF). In particular, FCS has also been used to gather information on the size of artificial lipid vesicles[24,25] and virus-like particles.[26] Here, we present a model-free analysis of the fluorescence fluctuations that circumvents the distortion of the ACF by highly fluorescent species in heterogeneous solutions by systematically measuring both duration and amplitude of each individual fluorescent event within the recorded time trace. The benefit of the single fluctuation analysis (SFA) is to provide in-depth distribution profiles of both size and membrane protein expression level, which are difficult to obtain by classical FCS. The combination of a highly efficient purification method with a single-molecule sensitivity detection technique enables here the characterization of the size distribution of EVs derived from cultured HEK293T cells and the relative expression level of the CD63 exosomal marker protein on the vesicles' surface.

RESULTS AND DISCUSSION

Extracellular vesicles released from HEK293T cells were collected and purified from conditioned medium (CM) as schematically described in Figure 1A. To avoid contamination by serum-derived EVs, the medium was replaced by serum-free medium 48 h before EV harvesting. Cell debris and large particles were removed from the CM using a 0.22 μm pore-sized filter. EVs were concentrated and simultaneously separated from parts of the soluble proteins present in the CM by UF over a 100 kDa molecular weight cutoff filter. While EVs are classically isolated by differential centrifugation,[14,15] our approach offers a rapid and simple way to obtain a concentrated solution of EVs still retaining their morphological integrity, as shown elsewhere for both cell culture media and body fluids.[7,8] We further purified EVs from residual soluble proteins using SEC. Elution profiles of a typical separation procedure of EVs immunostained with fluorescein-labeled antibodies against the exosomal marker CD63 (anti-CD63-FITC) are presented in Figure 1B. The absorbance chromatogram exhibited a small and well-resolved peak appearing at the void volume of the column and several broad peaks at larger elution volumes. The first peak in the void volume corresponded to the elution of the EVs with diameter wider than those of the pores in the Superose matrix, forcing them to pass straight through the column. The EVs were thus well separated from the remaining proteins and unbound antibodies as the latter were eluted in subsequent fractions. As a control, unlabeled EVs presented a similar absorbance chromatogram as shown in Figure S1A, Supporting Information. The fluorescence chromatogram exhibited a peak at the void volume together with a narrow peak appearing at a larger volume of elution. The first peak arose from the fluorescent antibodies specifically bound to the EVs, absent with unlabeled EVs (Figure S1A, Supporting Information) and pure antibodies (Figure S1B, Supporting Information), and an additional peak resulting from the elution of unbound antibodies. Furthermore, cryo-electron micrographs demonstrate that the integrity of the vesicles was preserved during the purification procedure: Figure 1C shows typical purified EVs as

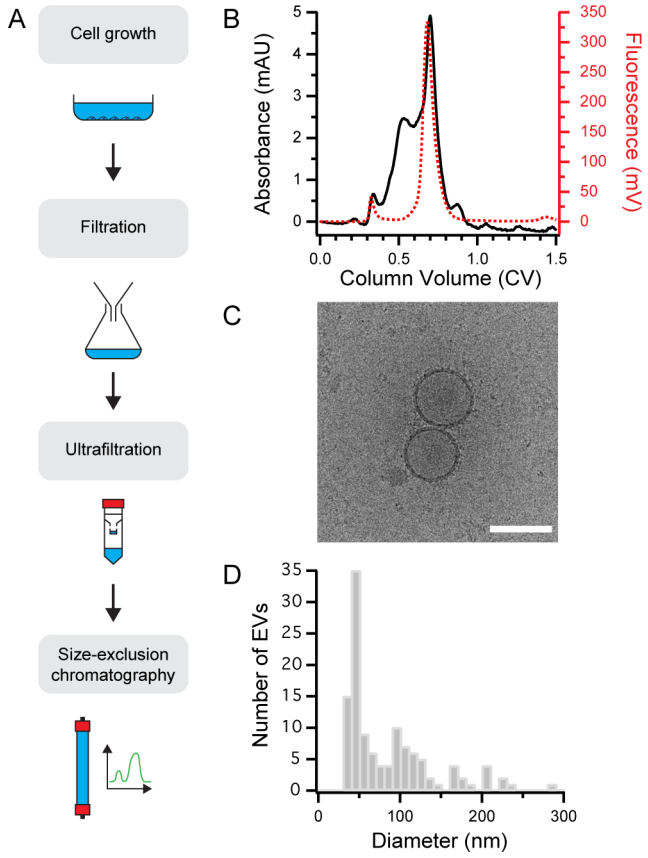

Figure 1. Purification strategy. (A) EVs were collected and purified from CM which was centrifuged and filtered with a 0.22 μm pore size filter in order to remove cell debris and big particles. UF prepurified and upconcentrated EVs while SEC further purified EVs from residual soluble proteins and organic molecules. (B) Typical SEC elution profile of EVs labeled with Anti-CD63-FITC, where absorbance at 280 nm (black solid line) monitors the global amount of proteins and the fluorescence (excitation at 485 nm, emission at 515 nm; red dashed line) indicates the presence of anti-CD63-FITC antibodies. The first peak at 0.33 CVs, visible in both spectra, corresponds to the specifically labeled EVs eluted in the void volume of the column and is well separated from the other peaks originating from soluble proteins. The sharp peak appearing at 0.7 CVs in the fluorescence chromatogram corresponds to the unbound antibodies. (C) Cryo-EM micrograph of purified EVs derived from HEK293T cells. Scale bar: 100 nm. (D) Size distribution of EVs obtained from cryo-EM samples analyzed with ImageJ software (NIH).

closed circular membrane vesicles ranging between 30 and 200 nm in diameter (Figure 1D).

Next, these purified immunolabeled EVs were analyzed by fluorescence fluctuation spectroscopy. Their translational diffusion through a diffraction-limited observation volume generated spikes in the recorded fluorescence time trace (Figure 2A,B). From the fluorescence intensity fluctuations over time, an ACF was evaluated as for FCS, which allows the estimation of average parameters such as concentration and size of the particles (Figure 2C). However, fluorescence brightness of an individual EV contributes in a quadratic fashion to the amplitude of the ACF,[27] biasing size estimation in highly heterogeneous samples. To circumvent this problem, we have systematically analyzed each translocation of individual labeled EVs through the confocal detection volume of our microscope (SFA). We developed an automatic routine which identified a translocation event when the fluorescence signal rose above a

dx.doi.org/10.1021/ac501801m | Anal. Chem. 2014, 86, 7229−7233

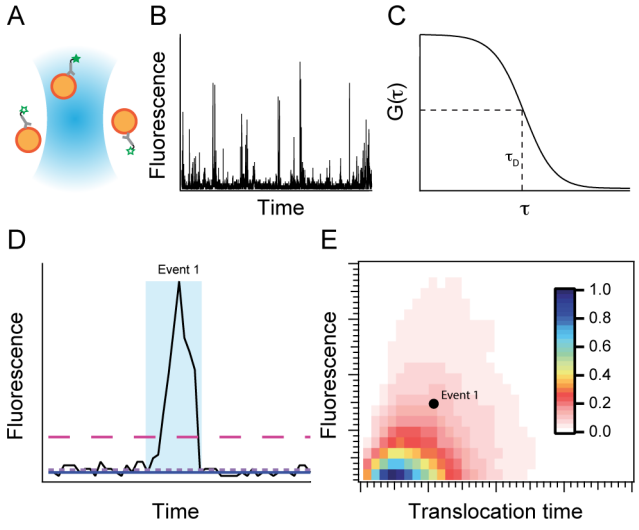

Figure 2. Scheme of model-free single fluctuation analysis. (A) A high-numerical aperture objective generates a femtoliter observation volume (blue) where vesicles (orange circles) fluorescently labeled with antibodies (green) are excited. (B) The recorded time trace contains distinct fluorescent spikes produced by Brownian diffusion of individual vesicle through the observation volume. (C) The fluorescence time trace can be classically analyzed with an ACF and an average translocation time τ_D can be deduced from various fitting models. (D) Alternatively, each spike is analyzed individually. The routine localizes events above a user-defined threshold (pink dashed line) with border points falling within 1.5× the standard deviation (violet dashed line) of the mean fluorescence signal (blue solid line) and extracts both maximal fluorescence intensity and translocation time (height and width of the light blue rectangular box, respectively). (E) The extracted parameters can be represented in a 2D-PDF of fluorescence intensity versus translocation time.

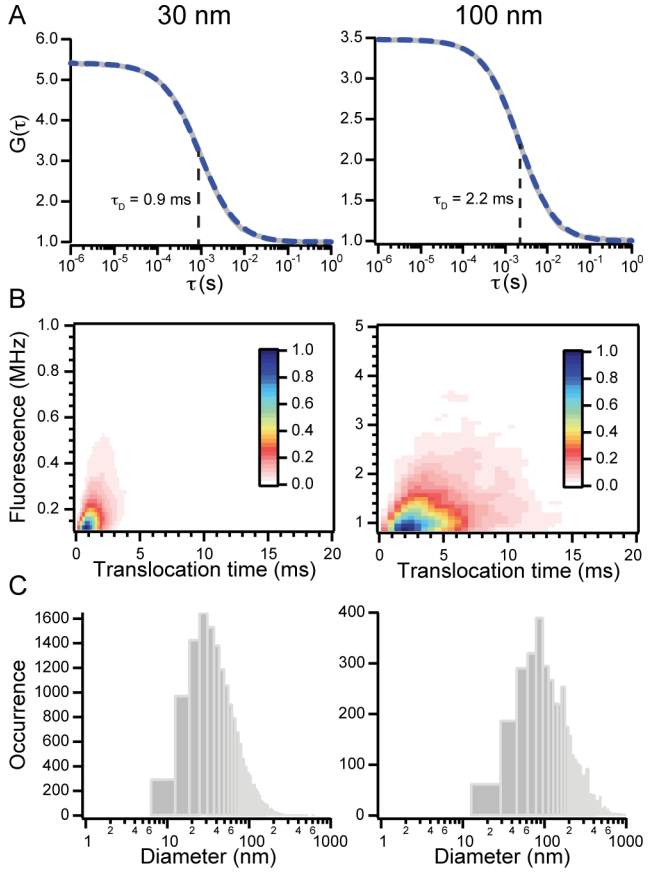

Figure 3. Fluorescence fluctuation spectroscopy of artificial lipid vesicles. (A) ACFs (gray solid lines) for the 30 and 100 nm vesicle preparations. The ACFs were fitted with a 3-dimensional 1-component diffusion model (blue dashed lines). (B) 2D-PDFs of fluorescence intensity versus translocation time for the two vesicle preparations obtained by SFA. (C) Histograms of the hydrodynamic diameters calculated from the data shown in (B).

user-defined threshold (Figure 2D, pink dashed line) which corresponded to a multiple of standard deviation of the fluorescence baseline (Figure 2D, blue solid line). For each identified translocation event, the fluorescence intensity was stored (Figure 2D, height of blue rectangular box) together with the translocation time which was defined as the time between the first and last points surpassing 1.5× the standard deviation (Figure 2D, width of blue rectangular box). Finally, these two parameters were represented in a 2-dimensional probability distribution function (2D-PDF, Figure 2E). In this approach, the smallest detectable particle is determined by the temporal resolution of the detector as well as the signal-to-noise ratio, while the upper limit is set by the Brownian motion. The detectable particle diameter ranges between 10 nm and 2−3 μm, which nicely covers the size distribution of EVs. To first test our methodology, we measured translocation of fluorescent vesicles of 30 and 100 nm prepared by mechanical extrusion. The fluorescence spikes contained in the time traces were analyzed according to both their ACF and 2D-PDF.

Fitting the ACFs by a 3-dimensional 1-component diffusion model yielded diffusion times of τ_D = 0.9 and τ_D = 2.2 ms, corresponding to average hydrodynamic diameters of D_H = 28 and D_H = 68 nm (Figure 3A). These values are slightly below those expected from the respective filter pores but are in good agreement with other reports.[28] On the other hand, SFA produced two distinct 2D-PDFs for the differently sized vesicles, concerning distribution of both translocation time and fluorescence intensity, reflecting correctly the characteristics of these vesicles (Figure 3B). The measured translocation times were then transformed into hydrodynamic diameters and presented as histograms of the size distribution of the EVs in Figure 3C. The most probable diameter (highest peak in the histogram) determined with our procedure corresponded to D_H = 24 and D_H = 77 nm for the 30 and 100 nm vesicles similar to what was obtained with classical FCS. More importantly, our methodology delivers in-depth information about the size and brightness distributions of the vesicles. Indeed, we observed a diameter range of 20−100 nm and 30−200 nm for 30 and 100 nm vesicles, respectively. The correspondence between the results obtained with our routine and the average parameters measured by classical FCS demonstrates its extreme accuracy. To further assess the precision of this analysis, we measured a polydisperse vesicle sample extruded through a 400 nm filter. The spread of the size distribution of this preparation was substantially larger compared to the 30 and 100 nm vesicle preparation (Figure S2A,B, Supporting Information). This broadening is in good agreement with data published elsewhere,[18] demonstrating that large-pore filters do not necessarily produce homogeneous preparations as small preformed vesicles pass through. Finally, the fluorescence intensity of a vesicle preparation scaled with the square of the vesicles diameter (0.1−0.3 MHz for 30 nm and 1−2 MHz for 100 nm), demonstrating that small vesicles recruit less fluorescent phospholipids in their bilayer due to their smaller

dx.doi.org/10.1021/ac501801m | Anal. Chem. 2014, 86, 7229−7233

total size. Deviation from linearity between fluorescence intensity versus translocation time (i.e., size) observed in the 2D-PDFs (Figures 3B and S2B, Supporting Information) is a consequence of sample polydispersity, reflecting compositional inhomogeneities as described elsewhere.[29]

We further applied our systematic analysis of individual fluorescence spikes in recorded time traces to a preparation of purified, immunostained EVs released from HEK293T cells. As free antibodies were removed by SEC, the background in the fluorescence time traces was extremely low which considerably improved the detection and characterization of EVs. Figure 4A

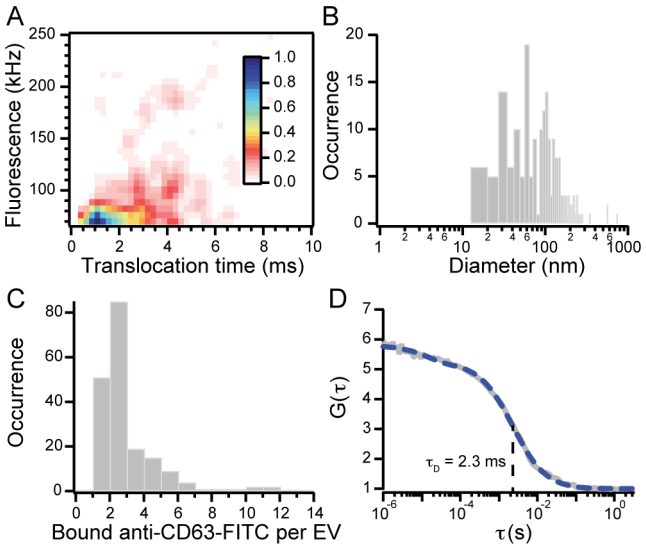

Figure 4. Fluorescence fluctuation spectroscopy of EVs released from HEK293T cells. (A) 2D-PDF of fluorescence intensity versus translocation time of EVs obtained by SFA. (B) Histogram of the calculated hydrodynamic diameter. (C) Histogram of the calculated number of bound anti-CD63-FITC per EV. (D) ACF (gray solid line) fitted with a 3-dimensional 1-component diffusion model taking into account the triplet state (blue dashed line).

presents the 2D-PDF of fluorescence intensity versus translocation time of cell-released EVs immunostained with anti-CD63-FITC. The distribution differed significantly from that of a pure antibody solution in the absence of EVs (Figure S3A,B, Supporting Information), demonstrating that our method allows the detection of the labeled vesicles. The vesicles had a most probable diameter of D_H = 56 nm (1.8 ms for the translocation time) with a size range of 30−200 nm as seen on the histogram of the size distribution (Figure 4B), which closely corresponded to what was determined by cryo-EM (Figure 1D). A superimposition of the two histograms (Figure S4, Supporting Information) indicates that SFA consistently reproduces the EV dimensional profile. Due to the extremely low fluorescence background of SEC purified EVs, SFA allows the detection of single fluorescently labeled membrane proteins in EVs. Thanks to the profile of the fluorescence intensity and the calculated mean fluorescence intensity of free antibodies (Figure S3C, Supporting Information), we determined the number of bound antibodies per EV, which ranged mainly from 1 to 6 with the most probability of 2 antibodies bound (Figure 4C). Hence, SFA can be used to determine, in addition to the vesicle size, the relative expression level of a particular membrane receptor in individual EVs. Finally, the average translocation time obtained from the fit of the ACF was τ_D = 2.3 ms (Figure 4D), only slightly above the most probable translocation time measured by our routine. This difference is explained by the presence of a small but bright EV subpopulation (centered at 200 kHz and 4 ms in the 2D-PDF, Figure 4A), which leads to a slight overestimation in FCS. The systematic analysis of the individual spikes in a fluorescence time trace thus provides reliable data on the dimensional and molecular distribution of EVs, when ACF fitting procedures fail due to the lack of information about particle brightness.

CONCLUSIONS

The combination of a proper purification/upconcentration protocol (UF and SEC) with a model-free fluorescence fluctuation analysis allowed a detailed and reliable characterization of molecular and dimensional distribution of EVs released from cultured cells. This novel two-step strategy provides ultrapure samples of EVs with preserved native properties, not only for single-vesicle analysis but also for studies where the absence of contaminants is of utmost importance (e.g., proteomics, RNA profiling, lipidomics). SEC keeps the morphology of the vesicles intact and provides information on the average expression level of particular membrane proteins when labeled with highly specific fluorescent antibodies. The combined SFA provides information on both vesicle size and membrane protein expression heterogeneities of the sample, which are characteristics hardly accessible simultaneously with classical techniques. The ability to analyze every single EV confers to our procedure an inherently higher spatial resolution than ensemble techniques, which suffer from intensity weighting bias. In addition, the actual size distribution of EVs is perfectly covered by the experimentally measurable range and the utmost sensitivity enables the detection of vesicles labeled with only a single fluorescent marker. Finally, our method benefits from reusable gel filtration columns and from fast data acquisition. Taken together, the current approach is ideally suited to become a standard for a reliable and robust multiparameter characterization of EVs.

ASSOCIATED CONTENT

Supporting Information

Additional information including experimental details and four supplemental figures. This material is available free of charge via the Internet at http://pubs.acs.org.

AUTHOR INFORMATION

Corresponding Author

*E-mail: horst.vogel@epfl.ch.

Author Contributions

#R.W. and L.G. contributed equally to this work.

Notes

The authors declare no competing financial interest.

ACKNOWLEDGMENTS

Financial support was provided by the Swiss National Science Foundation to H.V., L.G. and R.W. (System X − CINA and NCCR Chemical Biology), the European Community to H.V. and R.W. (project SynSignal, grant no. FP7-KBBE-2013-613879), Gebert Rüf Stiftung to L.G. and R.W. (GRS-038/13) and Marie Curie Actions to W.G. (SigT-OR-G).

REFERENCES

(1) Raposo, G.; Stoorvogel, W. *J. Cell Biol.* **2013**, *200*, 373−383.
(2) Mittelbrunn, M.; Sánchez-Madrid, F. *Nat. Rev. Mol. Cell Biol.* **2012**, *13*, 328−335.
(3) Rak, J. *Front. Pharmacol.* **2013**, *4*, 21.
(4) Buzás, E. I.; György, B.; Nagy, G.; Falus, A.; Gay, S. *Nat. Rev. Rheumatol.* **2014**, *10*, 356−364.
(5) Bellingham, S. A.; Guo, B. B.; Coleman, B. M.; Hill, A. F. *Front. Physiol.* **2012**, *3*, 124.
(6) El-Andaloussi, S.; Mäger, I.; Breakefield, X. O.; Wood, M. J. A. *Nat. Rev. Drug Discovery* **2013**, *12*, 347−357.
(7) Lamparski, H. G.; Metha-Damani, A.; Yao, J.-Y.; Patel, S.; Hsu, D.-H.; Ruegg, C.; Le Pecq, J.-B. *J. Immunol. Methods* **2002**, *270*, 211−226.
(8) Cheruvanky, A.; Zhou, H.; Pisitkun, T.; Kopp, J. B.; Knepper, M. A.; Yuen, P. S. T.; Star, R. A. *Am. J. Physiol. Renal Physiol.* **2007**, *292*, F1657−F1661.
(9) Lai, R. C.; Arslan, F.; Lee, M. M.; Sze, N. S. K.; Choo, A.; Chen, T. S.; Salto-Tellez, M.; Timmers, L.; Lee, C. N.; El Oakley, R. M.; Pasterkamp, G.; de Kleijn, D. P. V.; Lim, S. K. *Stem Cell Res.* **2010**, *4*, 214−222.
(10) Gercel-Taylor, C.; Atay, S.; Tullis, R. H.; Kesimer, M.; Taylor, D. D. *Anal. Biochem.* **2012**, *428*, 44−53.
(11) Davies, R. T.; Kim, J.; Jang, S. C.; Choi, E.-J.; Gho, Y. S.; Park, J. *Lab Chip* **2012**, *12*, 5202−5210.
(12) Chen, C.; Skog, J.; Hsu, C.-H.; Lessard, R. T.; Balaj, L.; Wurdinger, T.; Carter, B. S.; Breakefield, X. O.; Toner, M.; Irimia, D. *Lab Chip* **2010**, *10*, 505−511.
(13) Théry, C.; Amigorena, S.; Raposo, G.; Clayton, A. *Curr. Protoc. Cell Biol.* **2006**, DOI: 10.1002/0471143030.cb0322s30.
(14) Momen-Heravi, F.; Balaj, L.; Alian, S.; Mantel, P.-Y.; Halleck, A. E.; Trachtenberg, A. J.; Soria, C. E.; Oquin, S.; Bonebreak, C. M.; Saracoglu, E.; Skog, J.; Kuo, W. P. *Biol. Chem.* **2013**, *394*, 1253−1262.
(15) Witwer, K. W.; Buzás, E. I.; Bemis, L. T.; Bora, A.; Lässer, C.; Lötvall, J.; Nolte-'t Hoen, E. N.; Piper, M. G.; Sivaraman, S.; Skog, J.; Théry, C.; Wauben, M. H.; Hochberg, F. *J. Extracell. Vesicles* **2013**, *2*, 20360.
(16) van der Pol, E.; Coumans, F.; Varga, Z.; Krumrey, M.; Nieuwland, R. *J. Thromb. Haemostasis* **2013**, *11*, 36−45.
(17) Günter, M. *J. Bioanal. Biomed.* **2012**, *4*, 046−060.
(18) Kunding, A. H.; Mortensen, M. W.; Christensen, S. M.; Stamou, D. G. *Biophys. J.* **2008**, *95*, 1176−1188.
(19) Haustein, E.; Schwille, P. *Annu. Rev. Biophys. Biomol. Struct.* **2007**, *36*, 151−169.
(20) Hess, S. T.; Huang, S.; Heikal, A. A.; Webb, W. W. *Biochemistry* **2002**, *41*, 697−705.
(21) Wohland, T.; Friedrich, K.; Hovius, R.; Vogel, H. *Biochemistry* **1999**, *38*, 8671−8681.
(22) Grasso, L.; Wyss, R.; Piguet, J.; Werner, M.; Hassaine, G.; Hovius, R.; Vogel, H. *PLoS One* **2013**, *8*, No. e70929.
(23) Chmyrov, A.; Sandén, T.; Widengren, J. *J. Phys. Chem. B* **2010**, *114*, 11282−11291.
(24) Rusu, L.; Gambhir, A.; McLaughlin, S.; Rädler, J. *Biophys. J.* **2004**, *87*, 1044−1053.
(25) Rhoades, E.; Ramlall, T. F.; Webb, W. W.; Eliezer, D. *Biophys. J.* **2006**, *90*, 4692−4700.
(26) Chen, Y.; Bin, W.; Musier-Forsyth, K.; Mansky, L. M.; Mueller, J. D. *Biophys. J.* **2009**, *96*, 1961−1969.
(27) Lakowicz, J. R. *Principles of Fluorescence Spectroscopy*, 3rd ed.; Springer: New York, 2006.
(28) Hope, M. J.; Bally, M. B.; Webb, G.; Cullis, P. R. *Biochim. Biophys. Acta* **1985**, *812*, 55−65.
(29) Larsen, J.; Hatzakis, N. S.; Stamou, D. G. *J. Am. Chem. Soc.* **2011**, *133*, 10685−10687.